Metallic composites processed via extreme deformation: Toward the limits of strength in bulk materials

Dierk Raabe, Pyuck-Pa Choi, Yujiao Li, Aleksander Kostka, Xavier Sauvage, Florence Lecouturier, Kazuhiro Hono, Reiner Kirchheim, Reinhard Pippan, and David Embury

We review microstructures and properties of metal matrix composites produced by severe plastic deformation of multiphase alloys. Typical processings are wire drawing, ball milling, roll bonding, equal-channel angular extrusion, and high-pressure torsion of multiphase materials. Similar phenomena occur between solids in frictional contact such as in tribology, friction stir welding, and explosive joining. The resulting compounds are characterized by very high interface and dislocation density, chemical mixing, and atomic-scale structural transitions at heterointerfaces. Upon straining, the phases form into nanoscaled filaments. This leads to enormous strengthening combined with good ductility, as in damascene steels or pearlitic wires, which are among the strongest nanostructured bulk materials available today (tensile strength above 6 GPa). Similar materials are Cu-Nb and Cu-Ag composites, which also have good electrical conductivity that qualifies them for use in high-field magnets. Beyond the engineering opportunities, there are also exciting fundamental questions. They relate to the nature of the complex dislocation, amorphization, and mechanical alloying mechanisms upon straining and their relationship to the enormous strength. Studying these mechanisms is enabled by mature atomic-scale characterization and simulation methods. A better understanding of the extreme strength in these materials also provides insight into modern alloy design based on complex solid solution phenomena.

Introduction

Metal matrix composites with high interface density are produced via severe plastic co-deformation of multiphase alloys.[1–15] Corresponding compounds are first prepared by liquid or powder metallurgy[3–12] or through restacking solids of different composition.[2] Subsequent extreme straining, to promote intense microstructure refinement, proceeds by wire drawing, ball milling, accumulative roll bonding, damascene forging, equal channel angular extrusion, friction, or high-pressure torsion.[7]

Corresponding material systems can be grouped according to a microstructural or chemical classification scheme: From a microstructural perspective, multiphase systems can be classified as either particle-like alloys after primary syn-thesis or as lamellar or filament-type micro- or nanostructured materials. Often there is a transition between the two, for example, from a second phase with particulate initial shape into a deformation-induced lamellar and nanograined filament composite structure, such as in Cu-Nb, Cu-W, Cu-V, or Cu-Cr.[2–20] In other cases, the architecture is not changed during deformation, as in the case of pearlite,[1,21–28] where basic topological changes such as fiber curling occur only at very high strains.

From a chemical perspective, these alloy systems can be classified as immiscible pure-metal–metal-matrix compounds, intermetallic–metal-matrix compounds, or carbide–metal-matrix composites. In pure metal–metal-matrix composites, we observe the formation of supersaturated solid solutions[14]

Dierk Raabe, Max-Planck-Institut für Eisenforschung in Düsseldorf, Germany; d.raabe@mpie.de
Pyuck-Pa Choi, Max-Planck-Institut für Eisenforschung in Düsseldorf, Germany; p.choi@mpie.de
Yujiao Li, Max-Planck-Institut für Eisenforschung in Düsseldorf, Germany; y.li@mpie.de
Aleksander Kostka, Max-Planck-Institut für Eisenforschung in Düsseldorf, Germany; a.kostka@mpie.de
Xavier Sauvage, Institut de Physique at the University of Rouen, France; xavier.sauvage@univ-rouen.fr
Florence Lecouturier, Laboratoire National des Champs Magnétiques Intenses at CNRS, Toulouse, France; florence.lecouturier@lncmi.cnrs.fr
Kazuhiro Hono, National Institute for Materials Science in Sengen, Tsukuba, Japan; kazuhiro.hono@nims.go.jp
Reiner Kirchheim, Materials Physics Institute at the University of Göttingen; rkirch@ump.gwdg.de
Reinhard Pippan, Erich Schmid Institute in Leoben, Austria; reinhard.pippan@oeaw.ac.at
David Embury, McMaster University, Hamilton, Canada; emburyd@univmail.cis.mcmaster.ca

and sometimes small amorphous zones.[19] In the case of composites consisting of inter-metallics or carbides dispersed in a metallic matrix, one can additionally observe phase changes (from an ordered to a disordered phase or from crystalline to amorphous).[27–32]

Mechanical alloying to non-equilibrium solid solutions and deformation-driven as well as solid-solution-driven solid-state amorphization phenomena occur preferentially at heterophase interfaces. In cases where extreme strains are imposed, such as in ball milling, initially separate phases can nearly entirely dissolve into the matrix so that the multiphase character is lost.[14–34] In addition, severe wire drawing of multiphase alloys can lead to complex curling, where the minority phase forms into flat filaments that are bent about their longitudinal axis.

In general, different processes and alloy variants may lead to differences in nanostructure, amorphization, and mechanical alloying. The most essential criteria to identify whether a certain process and material combination tends to undergo preferential deformation-induced amorphization and/or mechanical alloying are the maximum attainable strain, the mutual solubility of the elements in each phase, the mixing energies of the elements stemming from the abutting phases, and the size difference of the solute atoms that enter the other phase during mechanical alloying.

Originally, the main interest in such heavily co-deformed compounds was to design materials with enormous interface-related strengthening combined with good ductility. For instance, multiply re-stacked damascene steels or heavily strained pearlite, such as that used in steel cord and piano wires, are among the strongest nanostructured bulk materials available today, with more than 6 GPa tensile strength (**Figures 1–3**). Wire-drawn Cu-20 wt% Nb alloys reveal up to 1.8 GPa strength combined with good electrical conductivity.[7,9]

Beyond the engineering opportunities (such as shown in Figure 1), a number of fundamental questions arise when driving composites toward the limits of strength through extreme deformation. These questions relate to the nature of the complex dislocation, amorphization, and mechanical alloying mechanisms that occur upon straining.[25–55] Studying these mechanisms has been recently enabled through matured atomic-scale characterization (e.g., atom probe tomography and high-resolution transmission electron microscopy) and simulation methods (e.g., molecular dynamics with improved potentials).

In this article, we give an overview of deformation microstructures and the resulting mechanical properties
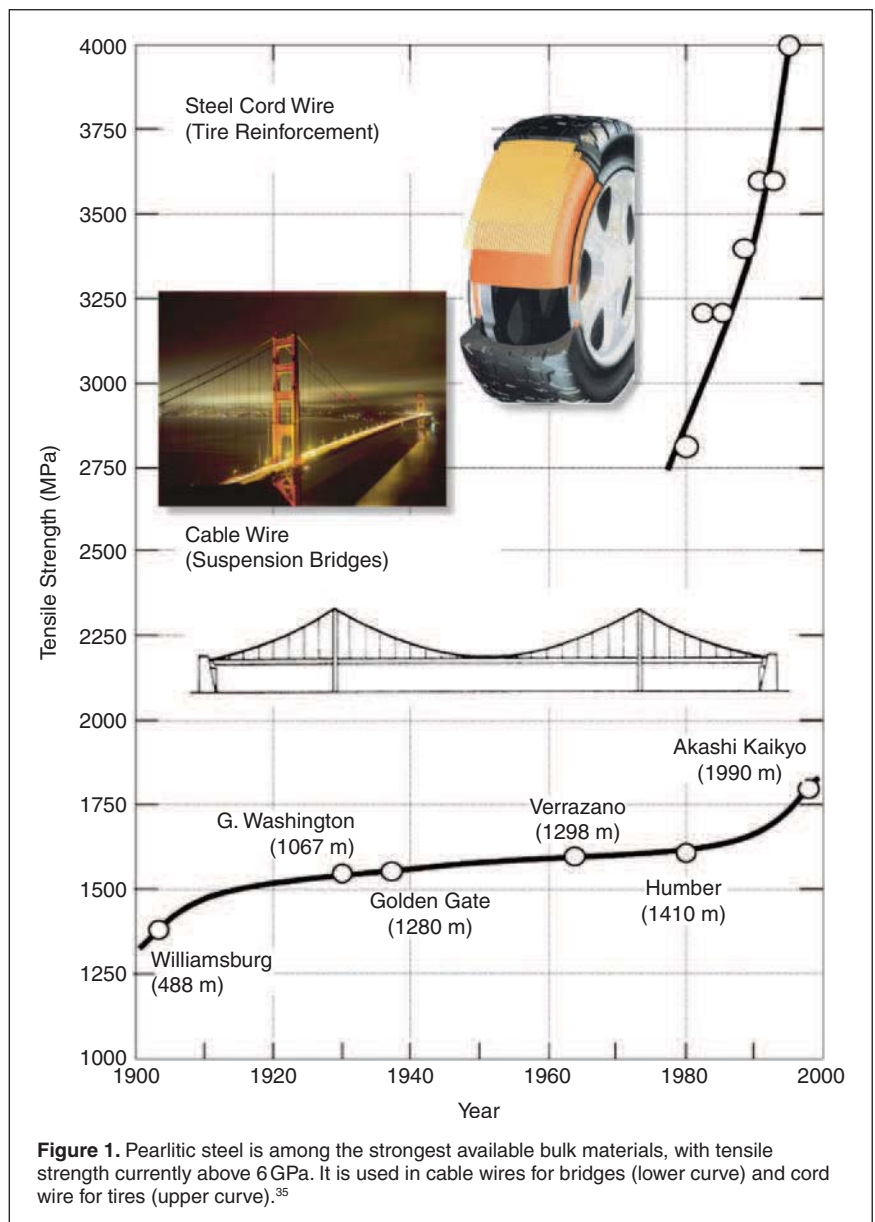

Figure 1. Pearlitic steel is among the strongest available bulk materials, with tensile strength currently above 6 GPa. It is used in cable wires for bridges (lower curve) and cord wire for tires (upper curve).[35]

obtained by extreme straining (true strains of 3–6, in some cases even up to 10). The aim is to identify microstructure features that are common to a number of different material combinations and processing conditions, including not only extreme bulk co-deformation but also nanotribology and frictional joining, as they reveal similar degrees of heavy local co-deformation. The main similarity among these different systems is that extremely strained heterophase interface areas are involved in all cases. In these regions, profound similarities can be observed in terms of the active mechanisms that may finally lead to interface-related plasticity, structural transitions (e.g., amorphization), atomic-scale mechanical alloying, phase formation, and phase decomposition.

Characteristic to all of these processes is that they lead to a certain degree of deformation-driven microstructure

hierarchy. This means that upon increasing co-deformation, a sequence in the microstructure evolution and also in the corresponding microstructure-property relations appears. The sequence of mechanisms generally does not follow the same strain dependence. However, as a rule, at low strains (micrometer spacing of interfaces), dislocation-based Orowan loop expansion and Hall-Petch mechanisms at the interfaces prevail, while at large strains (nanometer spacing of interfaces), dislocation-assisted atomic-scale processes through the interfaces determine the evolution of microstructure and strength. More specifically, in the nanoscopic regime, a number of mechanisms play a role, including structural decomposition, dislocation source size limitation, interface dislocation reactions, internal stresses, mechanically driven alloying across heterophase boundaries, and phase decomposition.
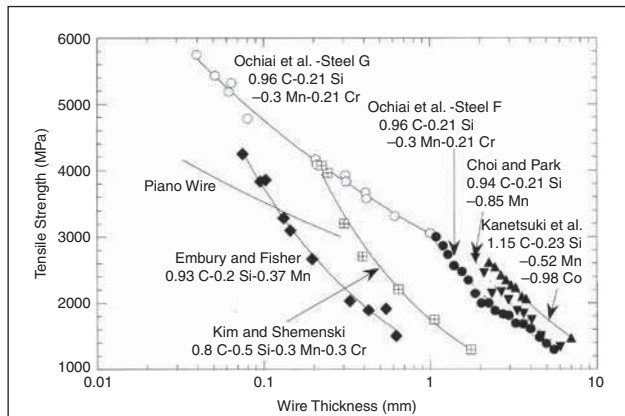

Figure 2. Tensile strength as a function of wire diameter during the wire drawing process for eutectoid and hypereutectoid pearlitic steels. Data are taken from Reference 27.
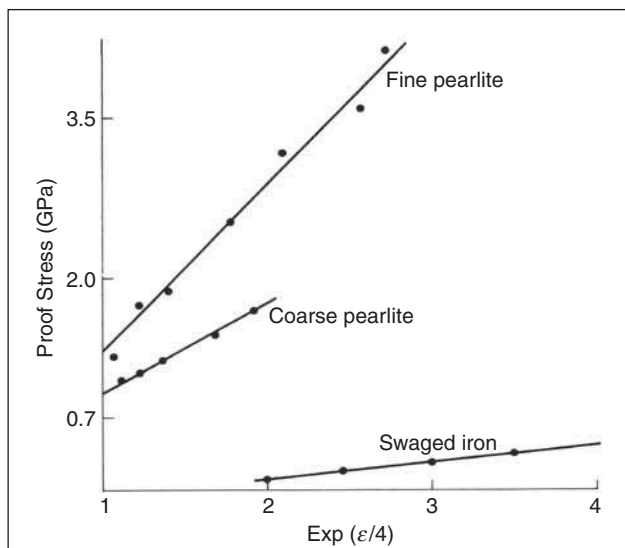

Figure 3. Variation of proof stress (stress at 0.2% plastic strain) with exp($\varepsilon/4$), where ε is the true strain for drawn pearlite and swaged iron.[1]

As an example, **Figure 4** shows results from atom probe tomography, where in a two-phase Fe-5 at.% Cu alloy with a large miscibility gap, the individual phases gradually start to dissolve under intense deformation obtained via ball milling.[51–53] The initial two-phase sample, analyzed after two hours, has not yet been completely mixed at an atomic scale (Figure 4a). Besides regions in which Cu atoms are dissolved in the Fe matrix, some Cu-rich fragments still exist. These fragments are formed by repeated fracture and cold-welding processes of powder particles trapped between colliding balls. After 20 h ball milling, no Cu-rich fragments appear (Figure 4b). The Cu atoms are nearly homogeneously distributed in the Fe matrix.

Of particular interest in this context is the question why extremely co-deformed composites still reveal very high and further increasing strength, although, in most cases, the interfaces are gradually dissolved and hence lose their separating function between the initial phases. This aspect will be discussed in the final section. This article is structured following the microstructure hierarchy, placing attention first on the extreme co-deformation of metal matrix composites
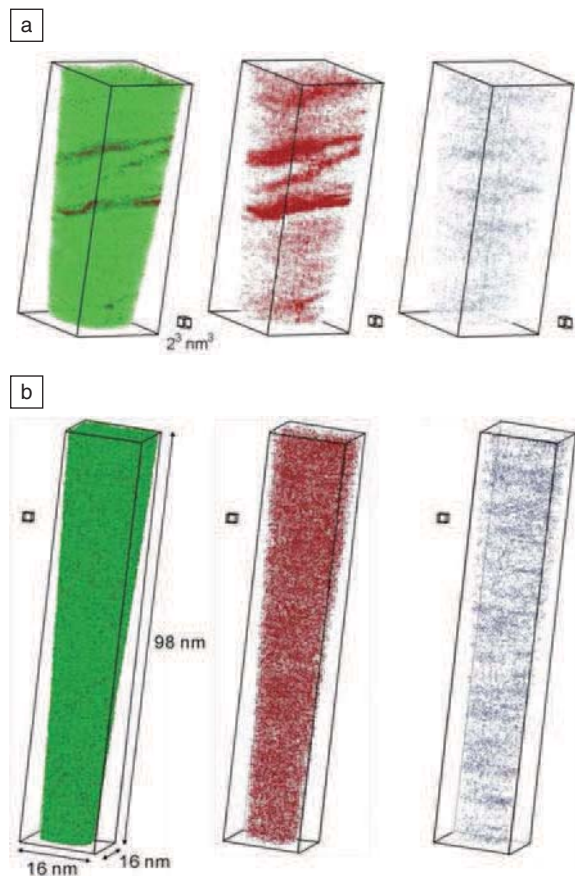

Figure 4. Atom-probe tomography data for $Fe_{95}Cu_5$ alloy ball-milled in a high-energy planetary ball mill. Fe atoms: green, Cu atoms: red, and O atoms: blue. Volume of small cube: $2 \times 2 \times 2$ nm³. (a) After 2 h.[48–50] (b) After 20 h.[51–53] The data reveal that the initial two-phase Fe-Cu alloy is rendered completely chemically mixed after heavy deformation in the ball mill after 20 h.

and subsequently on similar heterophase interface phenomena that play a role in the field of tribology and friction-dominated joining.

Hardening mechanisms of co-deformed composites: The micrometer scale

Metallic composites exposed to severe co-deformation go through a sequence of complex microstructure refinement phenomena. At low and average strains, the coexisting phases undergo a shape reduction that is related to the externally imposed strain, although usually not at a one-to-one relation, as the harder phases deform less than the matrix. Exceptions apply when the material undergoes necking and shear banding, where the harder phase can also be severely strained. This mesoscopic refinement reduces the average phase spacing. The interphase distance and the phase thickness determine the mean free path of the lattice dislocations at these scales, which governs the Hall-Petch hardening that is mainly responsible for the compound strength in this regime.

A simple microstructure-property relationship for the strength of wire-drawn pearlite can be formulated through a geometric model, where we assume by similitude that the strain-induced phase boundary spacing, d, and the external wire diameter, D, are proportional:

$$\frac{d_0}{d(\varepsilon)} = \frac{D_0}{D(\varepsilon)}, \tag{1}$$

where the "0" subscript indicates the initial value and the true strain ε is defined by

$$\varepsilon = 2\ln\left(D_0 / D(\varepsilon)\right). \tag{2}$$

Thus, if we assume a Hall-Petch scaling law, the stress σ is given by

$$\sigma(\varepsilon) = \sigma_0 + \frac{k}{\sqrt{d_0}}\exp\left(\frac{\varepsilon}{4}\right), \tag{3}$$

with a material-dependent strengthening coefficient k. Experimental results confirm the proportionality of proof stress (stress at 0.2% plastic strain) to the quantity $\exp(\varepsilon/4)$ for drawn pearlite and for swaged iron (Figure 3).

Upon further reduction in the interphase spacing, conventional bulk plasticity becomes less relevant for further increase in strength. This means that dislocation-dislocation interactions within the constituent phases and the Hall-Petch effect are gradually replaced by three effects, namely, limitations in activating dislocation sources, dislocation reactions at the heterointerfaces, and Orowan expansion of dislocations within the lamellae. Also, it was observed by many researchers[9,14,16,23,29,30,36,42] that very high dislocation and vacancy densities can be stored in this regime, **Figure 5**. For Cu-Nb nanocomposites, these mechanisms were studied in detail by a number of groups.[6–17,20,54] The dominating plastic deformation
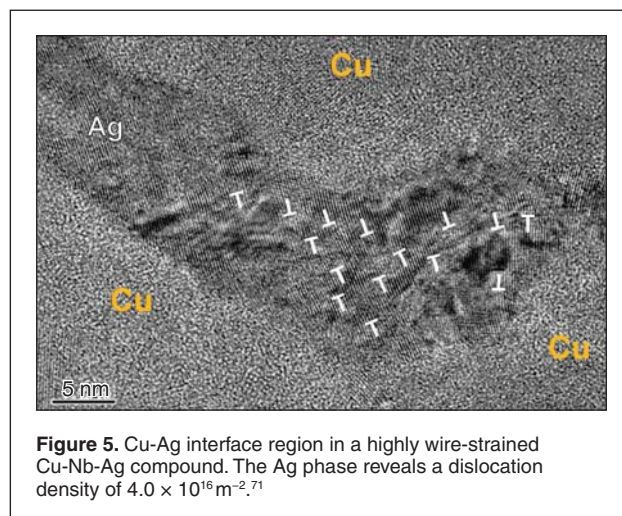

Figure 5. Cu-Ag interface region in a highly wire-strained Cu-Nb-Ag compound. The Ag phase reveals a dislocation density of $4.0 \times 10^{16}\,\mathrm{m}^{-2}$.[71]

mechanism in this material is the nucleation of single dislocation loops expanding in closely spaced parallel planes (Orowan mechanism) between Nb fibers, which behave as whiskers with an elevated elastic limit. Postmortem studies identified the dislocations involved in the process and revealed their role as associated defects at the complex Cu/Nb interfaces. As deformation proceeds, the number of loops increases, thus decreasing the distance between the loops on parallel planes.[54] When the number of dislocations at the interface is sufficient to accommodate the misfit between Cu and Nb, the mechanism stops. Pearlitic steels often start to deform plastically via the Orowan mechanism at low strains, since their starting microstructure is already very fine, with a typical interlamellar spacing of about 100 to 200 nm.[7,9,17,44,55]

Upon further microstructure refinement, dislocation penetration effects start to occur through heterointerfaces (even among non-coherent phases). Such heterophase slip transfer effects probably occur not only in the form of single-slip transition effects but also in the form of localization effects across interfaces by micro- or shear bands.[28–32]

Heterophase interface mechanics: Slip transmission and internal stresses

When the microstructure refinement reaches a level where intraphase dislocation multiplication and motion become geometrically impeded, slip transmission across the heterointerfaces starts to gain momentum. Embury[56] and Bieler[57] suggested criteria that promote slip transfer across interfaces. First, the resolved shear stress of the dislocations at the interface should be highest on the activated system. Second, the misorientation between the active slip planes on either side of the interface should be at a minimum at the boundary. Third, the configuration at the interface should be one of minimum energy. Another criterion is the ability for co-deformation of the abutting phases. In this context, the yield stress difference and ductility of both phases are important. Moreover, size effects could play a role, such as in the Fe-C system, where coarse pearlite cannot be

easily drawn because cementite is brittle, while fine pearlite can be well co-deformed, such as in steel cord[1,21–28] (Figures 1, 2, and 3).

In Cu-based alloys such as Cu-Ag or Cu-bcc (bcc: Nb, W, V, Mo, Cr, Fe), the criteria outlined previously are often fulfilled for the co-deformation of the two fcc phases Cu and Ag, as both materials form similar textures,[7,9] promoting a higher degree of orientation coherency (i.e., the orientations of the highly stressed slip systems match). Further examples of through-interphase slip transfer exist for Cu-Zr, α-β brass, and Ni-W. The bcc materials such as Nb or V often form textures that reveal Kurdjumov–Sachs coincidence between the leading slip systems in the bcc material and the corresponding systems in the fcc Cu.[7,9,17]

Dislocation slip across heterophase interfaces becomes active at high flow stresses and nanoscale fiber diameters because fibers with a micrometer-scale diameter can be deformed by regular dislocation multiplication and glide mechanisms. Slip transmission across the interface will create residual interface dislocations that may rearrange by glide or climb. Wang et al.[49,50] published atomistic and elasticity predictions that suggest that inbound lattice dislocations may preferably enter the interface rather than penetrating through it.

These simulations and experimental hints imply three important points regarding the consequences of interphase slip transfer: First, dislocation slip across an interface does not only represent an elementary unit of shear that is carried into the neighboring phase, but it represents an elementary step in chemical mixing across a heterophase-interface. Second, the fact that misfit dislocation debris may remain inside the interface initiates a structural rearrangement of the interface structure. Third, such mechanisms can lead to substantial internal stresses.[35,58] In Cu alloys with small Cr filaments, Embury and Sinclair showed that during the flux of dislocations across the interface between Cu and Cr, each slip transfer event leaves a residual misfit amount of shear and, hence, an unbalanced plastic transphase strain rate.[47,56,57] This effect leads to the buildup of an unrelaxed elastic strain and an additional hardening rate that is proportional to the shear transmission, the volume fraction, and the elastic modulus of the Cr phase. At large plastic strains, the internal strains developed in the two phases[34,58] result in an extended elastic-plastic transition and dimensional instability (**Figure 6**).[59,60]

These three aspects show that large straining of polyphase metallic alloys with slip transfer among co-deforming phases profoundly changes the chemistry, the crystallography, and the internal atomistic structure of heterointerfaces, when the inter-lamellar spacing becomes so small that intraphase dislocation motion and multiplication is impeded.

Mechanical alloying at heterophase interfaces: The atomic scale

One observation that is common to all heavily co-deformed metallic multiphase alloys (composites, tribology, frictional joints) is the phenomenon of mechanical alloying.[14,22,28,51–53]
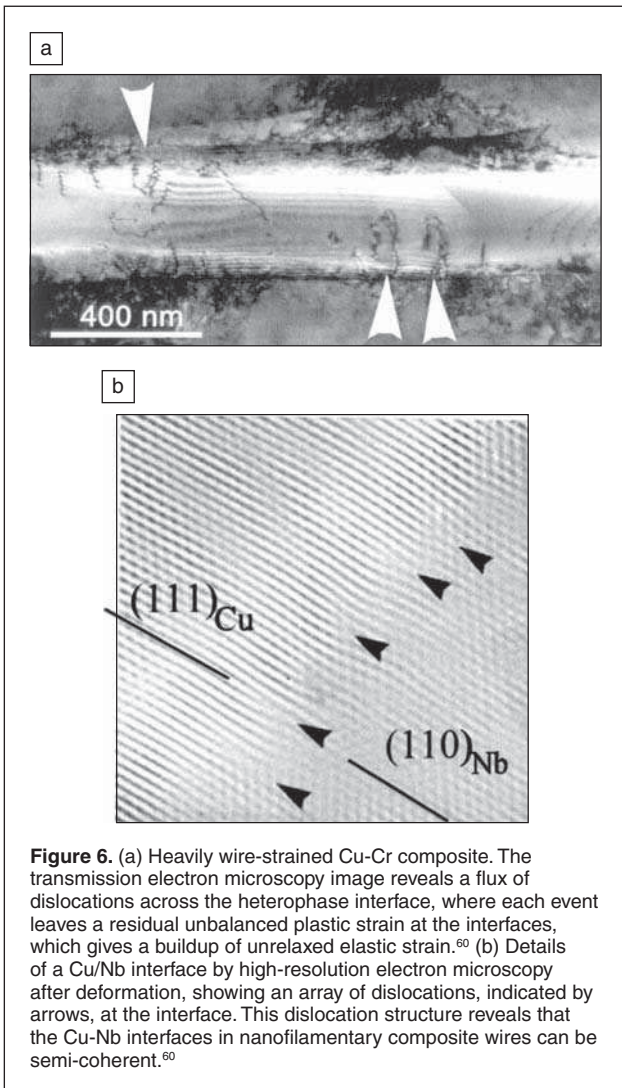
Figure 6. (a) Heavily wire-strained Cu-Cr composite. The transmission electron microscopy image reveals a flux of dislocations across the heterophase interface, where each event leaves a residual unbalanced plastic strain at the interfaces, which gives a buildup of unrelaxed elastic strain.[60] (b) Details of a Cu/Nb interface by high-resolution electron microscopy after deformation, showing an array of dislocations, indicated by arrows, at the interface. This dislocation structure reveals that the Cu-Nb interfaces in nanofilamentary composite wires can be semi-coherent.[60]

This means that multiphase materials with limited mutual solid-state solubility undergo plasticity-stimulated chemical mixing to levels far beyond equilibrium solubility. In many cases, this phenomenon leads to the complete dissolution of the minority phase into the matrix phase (Figure 4).

Mechanical alloying was observed in pearlite[24,25,27] and in various Cu-alloys after heavy straining (e.g., milling, drawing, rolling, torsion).[14,22,28,51–53,61–64] These observations raise two important issues. The first one is why massive mixing across heterointerfaces occurs among materials that usually reveal much smaller equilibrium mutual solubility. The second one is whether strengthening in such alloys at higher strains is based on phase boundaries or only on zones of local high strength (e.g., through layers of strong directional bonding). The latter question is particularly relevant, as some systems, such as pearlite wire, reveal the highest tensile stresses at large wire deformations, where the cementite phase has been nearly dissolved (i.e., where the original phases and sharp interfaces no longer exist).[22,28,61] Instead, the former interface regions are rendered into diffuse, chemically graded mechanically alloyed

zones, where strengthening more likely results from these solute effects rather than from sharp-interface mechanics (**Figure 7**).[64] For instance, for drawn pearlite, it is usually sufficient to impose true strains of 3, 4, or 5 to achieve a nanoscaled structure, cementite decomposition, and high strength. When drawing further, the strength increases, although the cementite has—to some extent—already dissolved, so that sharp interfaces can no longer play a dominant role for the strength.

In the following section, we discuss mechanically induced mixing in more detail. Various explanations were suggested to understand forced chemical mixing during co-deformation of phases consisting of non-soluble elements. The first one assumes a purely diffusion-driven mechanism.[65,66] The second one assumes defect-enhanced diffusion (dislocations, vacancies).[67,68] The third one is mainly built on interface roughening and plasticity-driven mechanical mixing (followed by subsequent short-range diffusion) via shear transfer (dislocations, shear bands) across heterophase interfaces.[67–72] The latter mechanism is also referred to as dislocation shuffling.[71]

A purely diffusion-driven approach can be ruled out for explaining forced chemical mixing among multiphase alloys, with small mutual solubility owing to the absence of thermodynamic driving forces. Even under consideration of enhanced vacancy densities, capillary pressure (Gibbs–Thomson effect), and internal stresses, no negative mixing enthalpy among most of the Cu- and Fe-based systems studied so far is obtained. The absence of a sufficient driving force for spontaneous interdiffusion and phase dissolution is also evident from annealing experiments, which show that wire-drawn and mechanically alloyed metal-matrix composites undergo immediate de-mixing and coarsening rather than further diffusion-driven alloying.

The second group of approaches for explaining mechanical mixing is based on plasticity-assisted short-range diffusion.
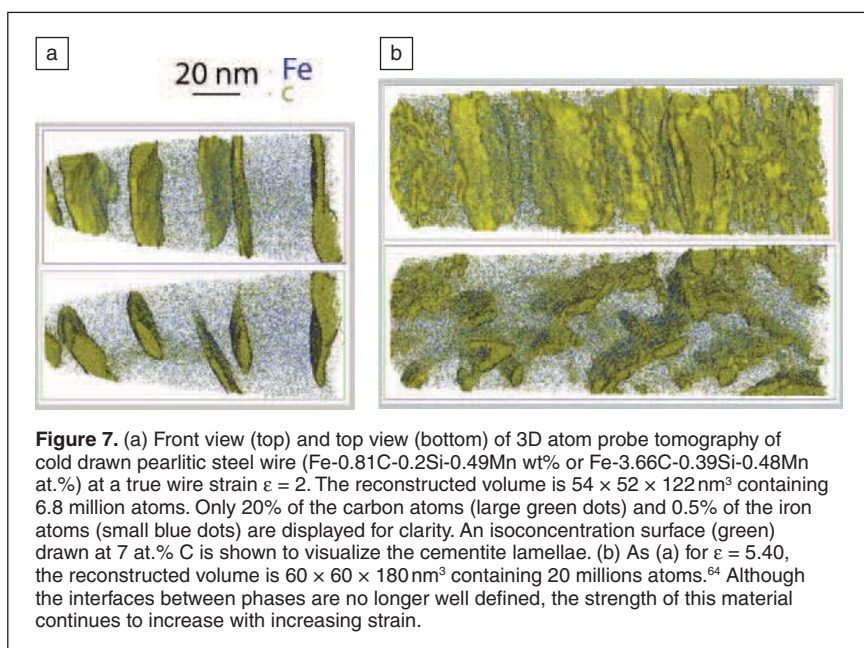
This mechanism attributes accelerated diffusion in binary systems to a deformation-induced increase in the non-equilibrium vacancy density. These additional diffusion carriers lead to chemical mixing across the interface. Although this effect is possible, one argument stands against it for explaining spontaneous alloying. All phases in a mechanically mixed alloy are plastically strained, though not to the same extent (i.e., an increased vacancy concentration is present in all phases). However, the excess vacancy concentration and their mobility do not have to be the same in all phases, so this could give rise to asymmetric diffusion gradients.

Hence, we conclude that deformation-stimulated increased diffusion is possible within the phases and also across the heterophase interfaces, but the net flux in either direction depends on the asymmetry in the defect densities and mobilities. Also, although diffusion across the interfaces is likely, it still cannot explain the massive non-symmetric interphase mixing observed,[71] because there are not sufficiently high thermodynamic driving forces.

A related mechanism of mechanical mixing is conceivable, though, in cases where the density of dislocations is so high that they attract larger quantities of solute atoms from the neighboring phase, owing to their high solubility. This effect is well known in the Fe-C system, where tertiary carbides dissolve as the C has a higher binding energy at the dislocation than within the carbide. Such an effect might also be responsible for the phenomenon that in heavily wire-drawn pearlite, strain aging after deformation leads to an increase in strength and loss in ductility. This mechanism is, however, not based on pipe diffusion or higher vacancy densities but on the higher solubility of dislocations for solutes.

In contrast to these mechanisms that are more driven by diffusion and enhanced defect solubility, it is also conceivable that transphase dislocation-assisted carrier mechanisms assist mechanically induced chemical mixing. This phenomenon is described by the dislocation-shuffle mechanism.[71] While elementary single-slip heterophase transmission effects, as described previously, can explain local structural changes of the interfaces and the buildup of internal stresses, corresponding multislip shear transfer (shear on more than one slip system) across heterointerfaces can lead to massive chemical mixing (**Figure 8**). Dislocation shuffling describes transphase plastic deformation on more than one slip system. Such shearing and interface roughening can create small embedded particles consisting of atoms from one phase in the other. Such tiny material portions can be further cut by dislocations running through them, thereby increasing their energy through the Gibbs–Thomson effect so that they finally dissolve.[71]

In a corresponding experiment with a thin multilayered starting microstructure consisting
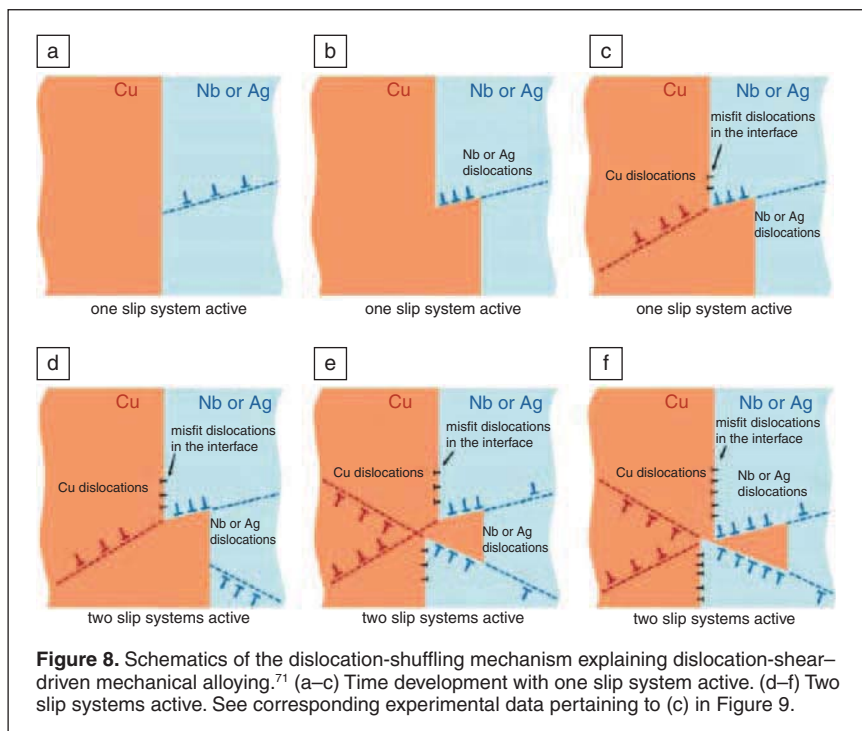

Figure 7. (a) Front view (top) and top view (bottom) of 3D atom probe tomography of cold drawn pearlitic steel wire (Fe-0.81C-0.2Si-0.49Mn wt% or Fe-3.66C-0.39Si-0.48Mn at.%) at a true wire strain $\varepsilon = 2$. The reconstructed volume is $54 \times 52 \times 122 \, nm^3$ containing 6.8 million atoms. Only 20% of the carbon atoms (large green dots) and 0.5% of the iron atoms (small blue dots) are displayed for clarity. An isoconcentration surface (green) drawn at 7 at.% C is shown to visualize the cementite lamellae. (b) As (a) for $\varepsilon = 5.40$, the reconstructed volume is $60 \times 60 \times 180 \, nm^3$ containing 20 millions atoms.[64] Although the interfaces between phases are no longer well defined, the strength of this material continues to increase with increasing strain.

Figure 8. Schematics of the dislocation-shuffling mechanism explaining dislocation-shear–driven mechanical alloying.[71] (a–c) Time development with one slip system active. (d–f) Two slip systems active. See corresponding experimental data pertaining to (c) in Figure 9.

of parallel Cu and V filaments, Sauvage[72] observed such an elementary shear event across the Cu/V interface (**Figure 9**a) (note that Figure 9a shows an unpublished analysis from a data set measured for Reference 72.) Similar effects were observed in Cu-Nb nanocomposites[71] and pearlite (Figure 9b).[14]

Deformation-driven amorphization
Extreme co-deformation of multiphase alloys or of bulk heterophases in frictional contact reveal, in some cases, deformation-driven amorphization phenomena. Two situations have been observed. First, some systems undergo amorphization without substantial non-equilibrium chemical mixing among the phases. In the field of multiphase co-deformation, this occurs for the Ni-Ti system, which undergoes amorphization if subjected to severe plastic deformation, but without substantial local composition change. This first group of systems obviously can be thermodynamically de-stabilized by a sufficiently high defect density without the contribution of compositional changes.

The second group comprises systems where solid-state amorphization is connected to the preceding formation of non-equilibrium solid solutions during deformation. This effect seems to occur particularly in composites with negative enthalpy of mixing. Typically, the pure bulk elements of the compounds addressed in this overview, such as Fe, Cu, Ag, and Nb, do not become amorphous when exposed to heavy straining as single phase bulk materials. This observation indicates that a relationship exists between mechanical alloying, the enthalpy of mixing of the newly formed compounds, and amorphization. This argument is also supported by the fact that the abutting phases in Fe and Cu compos-

ites frequently reveal very high dislocation densities, Figure 5. The relationship between mechanical mixing and amorphization seems to apply, in particular, to the Cu-matrix in Cu-Nb- or Cu-Zr-based composites and to the ferritic phase in pearlite. These matrix phases become amorphous only when mechanically alloyed. Deformation-induced amorphization of Cu during wire drawing was reported in Cu-Nb, Cu-Nb-Ag (Figure 8b), and Cu-Zr (**Figure 10**).[9,15,71,74–77] In all cases, at least one pair of the constituent elements reveal a negative enthalpy of mixing. Similar observations were reported on pearlitic wire at relatively low true strains as low as 1, although these observations are, in part, under debate.

For instance, according to the Gibbs free energy versus concentration diagram, amorphous Cu-Nb could be stable at 25°C, relative to the bcc and fcc solid solutions that could be formed by forced mixing, for Cu concentrations between 35 at.% and 80 at.%.[71,72] Most of the published Cu-Nb alloys where amorphization occurred fall in this regime. Similar results were observed in Cu-Zr, Figure 10.[71]

Another way to explain amorphization in severely deformed multiphase alloys is to consider the increase in the free energy due to dislocations.[66–71] If the stored deformation energy increases upon straining, it is conceivable that transformation into the amorphous regime is energetically favorable, Figure 5. This argument, however, is not fully convincing, because dislocations can be absorbed, in part, in the interfaces rather than being stored within the phases.[50,51,71]

Owing to these considerations, we suggest that amorphization takes place in co-deformed metallic composites in a two-step mechanism that consists of first, a dislocation-shuffling or shear-band-related transphase plastic deformation and chemical mixing process,[71,72] and second, a gradual amorphization in regions where both heavy mixing and high dislocation densities exist. The transition seems to be particularly likely in systems that fulfill at least some of the classical glass-forming rules. In systems that reveal amorphization without substantial chemical mixing, the effect is attributed to the large accumulated dislocation densities.

Microstructures and properties during frictional contact of heterointerfaces
Similar intense deformation conditions and metallurgical effects, as discussed for heavily co-deformed multiphase alloys, also occur at heterointerfaces between bodies that are brought in frictional contact such as encountered in tribology, friction stir welding, and explosive joining.[78–80] In these cases, the extreme deformation is localized at the interface regions (i.e., these materials do not undergo bulk deformation). However, at the interfaces that are in frictional contact, similar

Figure 9. (a) 3D atom-probe measurements on a vanadium filament embedded in a Cu matrix exposed to high-pressure torsion deformation sheared by a large number of dislocations (5 nm step). Only vanadium atoms are displayed. The observation indicates a possible dislocation-shuffling mechanism. The lower image shows vanadium concentration along two cross sections. The images were reproduced from raw data obtained from Reference 72. (b) Left: 3D atom probe reconstruction of a small volume of a Cu-Nb wire-deformed at 40 K. Copper atoms are represented in small grey dots, while large black dots correspond to niobium.[14,73] The arrows indicate possible transphase dislocation shear events, such as observed in (a) for Cu-V. Right: Similar case observed on a cementite-ferrite interface in a deformed pearlite wire.

Why do co-deformed composites have high strength after phase dissolution?

Takahashi discussed the upper limits of possible strengthening mechanisms that may theoretically determine the strength of severely strained composites.[22,24] The reasoning behind such estimates is the somewhat counter-intuitive observation that the strength of co-deformed compounds increases further with ongoing straining, even in cases where the original phases were dissolved via mechanical alloying. This means that the originally chemically sharp heterointerfaces are blurred and even gradually lost. Hence, in such cases, conventional strengthening based on a sharp and (mostly) incoherent interface cannot be responsible for the strength increase with further straining. Instead, real microstructures of severely deformed multiphase alloys are characterized by graded rather than sharp interfaces, and, in extreme cases, can even reveal entirely dissolved phases. In such cases, the matrix seems to be mainly hardened by high non-equilibrium fractions of solute atoms in the form of a mechanically driven solid solution and its effect on the Peierls potential and a high stored-dislocation content.

According to Takahashi, when considering eutectoid pearlite, the upper-bound strength that can be achieved by dislocation strengthening amounts to about 5 GPa. This value is given by the upper limit to the dislocation density that can be stored in the material. The upper limit of Hall-Petch and Orowan hardening through grain refinement is about 2 GPa. The upper strength limit given by a maximum amount of mechanically driven solid solution is about 0.5 GPa. This estimate seems to be a bit low, though, as it is based on the assumption of pure solid-solution hardening, and the high internal stresses created by an excess amount of interstitials is neglected in this balance. Finally, second-phase hardening gives an upper bound of 4 GPa. According to Takahashi, linear summation of these contributions would result in an upper bound of the strength of about 11.5 GPa. We do not suggest that this approach of describing the upper bound value for pearlite proof strength is exact, as the second phases gradually dissolve as just stated. Also, the contribution of the solid-solution strengthening could be higher owing to the fact that the cementite becomes strongly dissolved, providing a higher C content. Finally, the materials build up large internal stresses during severe deformation, which provides an additional source of strengthening. Irrespective of these points,
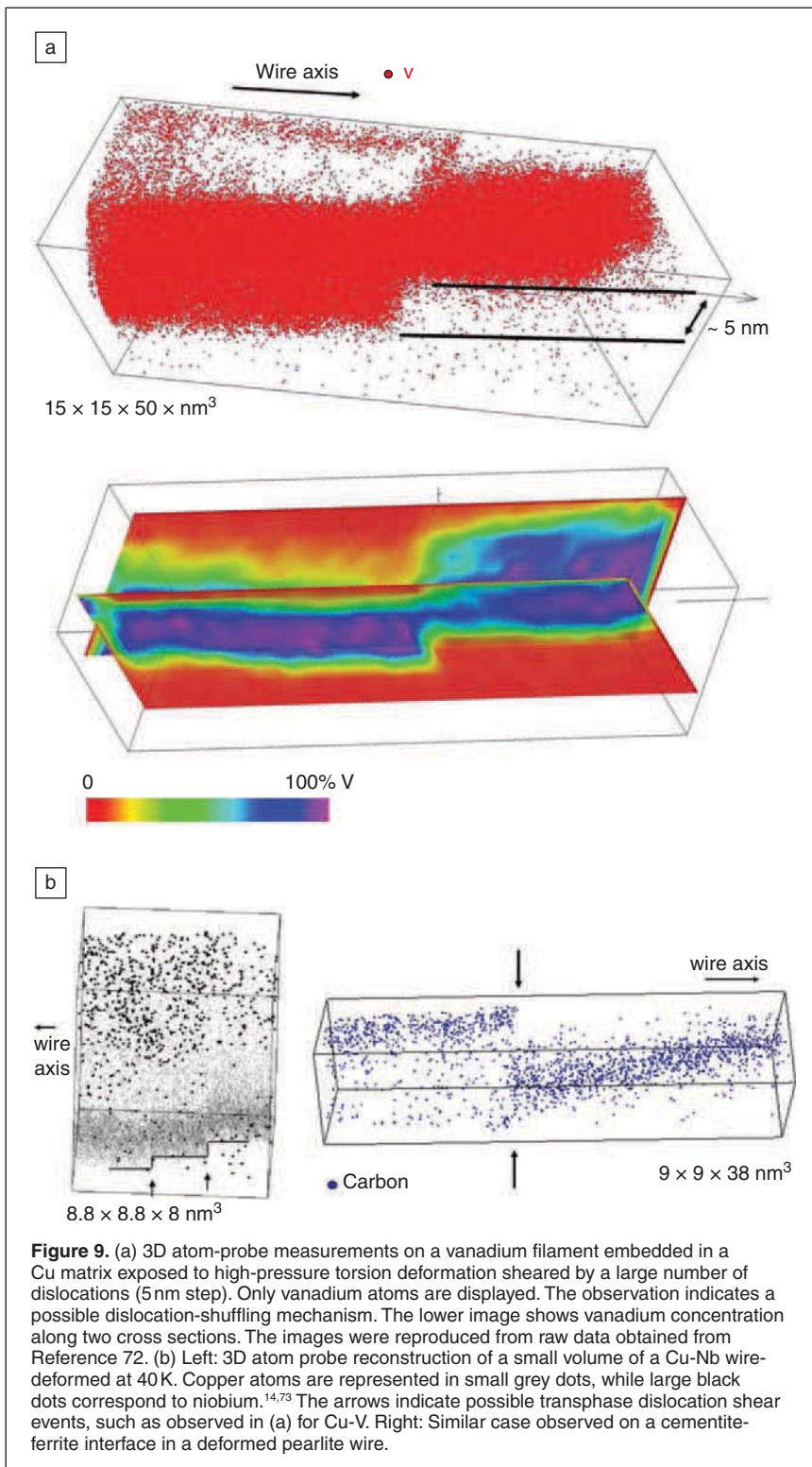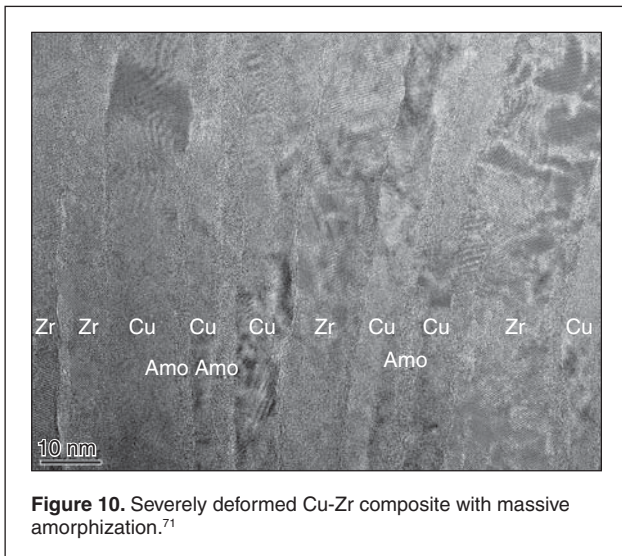
phenomena occur as in co-deformed composites, namely deformation-driven chemical mixing, amorphization, and very high accumulated dislocation densities. Hence, the interface regions of bulk co-deformed systems and tribological systems reveal phenomena of high similarity.

Figure 10. Severely deformed Cu-Zr composite with massive amorphization.[71]

the simple estimate reveals that several mechanisms other than the Hall-Petch effect can contribute to substantial strength in severely co-deformed composites.

Summary

Multiphase alloys can be rendered into ultrahigh strength bulk compounds by severe plastic co-deformation, which transforms the phases into nanoscaled filaments. At moderate and intermediate deformation, the microstructure is characterized by a high interface density. Strengthening in this regime is mainly due to Orowan and Hall-Petch effects. At high deformation, strengthening is determined by interface dislocation reactions, heterophase dislocation penetration, and high dislocation density. In this strain regime, intense deformation-driven chemical mixing (mechanical alloying) and atomic-scale structural transitions (e.g., amorphization) occur. For deformation-driven mixed systems with glass-forming characteristics (negative enthalpy of mixing), mechanical alloying and amorphization are considered to be associated phenomena. In mechanically mixed systems without the typical glass-forming tendency, structural transitions are attributed to the reduction of the high stored dislocation densities by amorphization. Among the various mechanisms that can lead to massive mechanical alloying, we suggest a dominant role for transphase dislocation shuffling or shear-band mechanisms, in which lattice dislocations penetrate the interfaces between abutting phases acting as carriers of deformation-driven chemical mixing. Heavily co-deformed multiphase materials offer an enormous potential for advanced alloy design. These materials today represent the largest class of ultrahigh strength nanostructured bulk materials.

References

1. J.D. Embury, R.M. Fisher, *Acta Metall.* **14**, 47 (1966).
2. F.P. Levi, *J. Appl. Phys.* **31**, 1469 (1960).
3. G. Frommeyer, G. Wassermann, *Acta Metall.* **23**, 1353 (1975).
4. J. Bevk, J.P. Harbison, I.L. Bell, *J. Appl. Phys.* **49**, 6031 (1978).
5. P.D. Funkenbusch, T.H. Courtney, *Acta Metall.* **33**, 913 (1985).
6. W.A. Spitzig, A.R. Pelton, F.C. Laabs, *Acta Metall.* **35**, 2427 (1987).
7. A.M. Russell, L.S. Chumbley, Y. Tian, *Adv. Eng. Mater.* **2**, 11 (2000).
8. M.H. Hong, W.T. Reynolds, Jr., T. Tarui, K. Hono, *Metall. Mater. Trans. A* **30**, 717 (1999).
9. D. Raabe, F. Heringhaus, U. Hangen, G. Gottstein, *Z. Metallkd.* **86**, 405 (1995).
10. D. Raabe, K. Miyake, H. Takahara, *Mater. Sci. Eng. A* **291**, 186 (2000).
11. F. Dupouy, S. Askénazy, J.P. Peyrade, D. Legat, *Phys. B* **211**, 43 (1995).
12. J.T. Wood, J.D. Embury, M. Ashby, *Acta Mater.* **45**, 1099 (1997).
13. J.D. Embury, K. Han, *Curr. Opin. Solid State Mater. Sci.* **3**, 304 (1998).
14. X. Sauvage, L. Thilly, F. Lecouturier, A. Guillet, D. Blavette, *Nanostruct. Mater.* **11**, 1031 (1999).
15. X. Sauvage, L. Renaud, B. Deconihout, D. Blavette, D.H. Ping, K. Hono, *Acta Mater.* **49**, 389 (2001).
16. L. Thilly, F. Lecouturier, J. von Stebut, *Acta Mater.* **50**, 5049 (2002).
17. F. Heringhaus, D. Raabe, G. Gottstein, *Acta Metall.* **43**, 1467 (1995).
18. Y. Sakai, K. Inoue, H. Maeda, *Acta Metall.* **43**, 1517 (1995).
19. Y. Sakai, H.J. Schneider-Muntau, *Acta Metall.* **45**, 1017 (1997).
20. F. Heringhaus, H.J. Schneider-Muntau, G. Gottstein, *Mater. Sci. Eng.* **347**, 9 (2003).
21. G. Langford, *Metall. Trans.* **8A**, 861 (1977).
22. T. Tarui, N. Maruyama, J. Takahashi, S. Nishida, H. Tashiro, *Nippon Steel Techn. Rep.* **91**, 56 (2005).
23. S. Goto, R. Kirchheim, T. Al-Kassab, C. Borchers, *Trans. Nonferrous Met. Soc. China* **17**, 1129 (2007).
24. J. Takahashi, T. Tarui, K. Kawakami, *Ultramicroscopy* **109**, 193 (2009).
25. A. Taniyama, T. Takayama, M. Arai, T. Hamada, *Scripta Mater.* **51**, 53 (2004).
26. K. Oh-ishi, H.W. Zhang, T. Ohkubo, K. Hono, *Mater. Sci. Eng. A* **456**, 20 (2006).
27. D.R. Lesuer, C.K. Syn, O.D. Sherby, D.K. Kim, in *Metallurgy, Processing and Applications of Metal. Wires,* H.G. Paris, D.K. Kim, Eds. (TMS, Warrendale, PA, 1996).
28. K. Hono, M. Ohnuma, M. Murayama, S. Nishida, A. Yoshie, T. Takahashi, *Scripta Mater.* **44**, 977 (2001).
29. S. Ohsaki, K. Yamazaki, K. Hono, *Scripta Mater.* **48**, 1569 (2003).
30. S. Ohsaki, K. Hono, H. Hidaka, S. Takaki, *Scripta Mater.* **52**, 271 (2005).
31. H.W. Zhang, S. Ohsaki, S, Mitao, M. Ohnuma, K. Hono, *Mater. Sci. Eng. A* **421**, 191 (2006).
32. S. Ohsaki, S. Kato, N. Tsuji, T. Ohkubo, K. Hono, *Acta Mater.* **55**, 2885 (2007).
33. H.R. Gong, B.X. Liu, *J. Appl. Phys.* **96**, 3020 (2004).
34. J.D. Embury, M.A. Hill, W.A. Spitzig, Y. Sakai, *MRS Bull.* **8**, 57 (1993).
35. M. Elices, *J. Mater. Sci.* **39**, 3889 (2004).
36. K. Spencer, F. Lecouturier, L. Thilly, J.D. Embury, *Adv. Eng. Mater.* **6**, 290 (2004).
37. E. Botcharova, J. Freudenberger, A. Gaganov, K. Khlopkov, L. Schultz, *Mater. Sci. Eng. A* **416**, 261 (2006).
38. G. Langford, *Metall. Trans.* **1**, 465 (1970).
39. C. Trybus, W.A. Spitzig, *Acta Metall.* **37**, 1971 (1989).
40. J.G. Sevillano, *J. Phys. III* **6**, 967 (1990).
41. U. Hangen, D. Raabe, *Acta Metall.* **43**, 4075 (1995).
42. D. Raabe, D. Mattissen, *Acta Mater.* **46**, 5973 (1998).
43. D. Raabe, D. Mattissen, *Acta Mater.* **47**, 769 (1999).
44. D. Raabe, U. Hangen, *Acta Metall.* **44**, 953 (1996).
45. A. Misra, J.P. Hirth, R.G. Hoagland, *Acta Mater.* **53**, 4817 (2005).
46. J.D. Embury, J.P. Hirth, *Acta Metall.* **42**, 2051 (1994).
47. J.D. Embury, C.W. Sinclair, *Mater. Sci. Eng. A* **319**, 37 (2001).
48. J.D. Embury, *Scripta Metall. Mater.* **27**, 981 (1992).
49. J. Wang, R.G. Hoagland, J.P. Hirth, A. Misra, *Acta Mater.* **56**, 5685 (2008).
50. J. Wang, R.G. Hoagland, J.P. Hirth, A. Misra, *Acta Mater.* **56**, 3109 (2008).
51. C. Wille, T. Al-Kassab, P.P. Choi, Y.S. Kwon, *Ultramicroscopy* **109**, 599 (2009).
52. C. Wille, T. Al-Kassab, M. Schmidt, P.P. Choi, Y.S. Kwon, *Int. J. Mater. Res.* **99**, 541 (2008).
53. P.P. Choi, T. Al-Kassab, Y.S. Kwon, J.S. Kim, R. Kirchheim, *Microsc. Microanal.* **13**, 347 (2007).
54. L. Thilly, O. Ludwig, M. Véron, F. Lecouturier, J.P. Peyrade, S. Askénazy, *Philos. Mag. A* **82**, 925 (2002).
55. M. Janecek, F. Louchet, B. Doisneau-Cottignies, Y. Bréchet, N. Guelton, *Philos. Mag. A* **80**, 1605 (2000).
56. C.W. Sinclair, J.D. Embury, G.C. Weatherly, *Mater. Sci. Eng. A* **272**, 90 (1999).
57. T.R. Bieler, P. Eisenlohr, F. Roters, D. Kumar, D.E. Mason, M.A. Crimp, D. Raabe, *Int. J. Plast.* **25**, 1655 (2009).
58. J.M. Atienza, J. Ruiz-Hervias, M.L. Martinez-Perez, F.J. Mompean, M. Garcia-Hernandez, M. Elices, *Scripta Mater.* **52**, 1223 (2005).
59. L. Thilly, S. Van Petegem, P.O. Renault, F. Lecouturier, V. Vidal, B. Schmitt, H. Van Swygenhoven, *Acta Mater.* **57**, 3157 (2009).

60. F. Dupouy, E. Snoeck, M.J. Casanove, C. Roucau, J.P. Peyrade, S. Askénazy, *Scripta Mater.* **34**, 1067 (1996).
61. C. Borchers, T. Al-Kassab, S. Goto, R. Kirchheim, *Mater. Sci. Eng. A* **502**, 131 (2009).
62. X. Sauvage, F. Wetscher, P. Pareige, *Acta Mater.* **53**, 2127 (2005).
63. J.Y. Huang, Y.D. Yu, Y.K. Wu, D.X. Li, H.Q. Ye, *Acta Mater.* **45**, 113 (1997).
64. Y.J. Li, P. Choi, C. Borchers, Y.Z. Chen, S. Goto, D. Raabe, R. Kirchheim, *Acta Mater.* (2010), in press.
65. J. Eckert, J.C. Holzer, C.E. Krill III, W.L. Johnson, *J. Appl. Phys.* **73**, 2794 (1993).
66. J. Eckert, J.C. Holzer, C.E. Krill III, W.L. Johnson, *J. Mater. Res.* **1992**, 7 (1980).
67. E. Ma, H.W. Sheng, J.H. He, P.J. Schilling, *Mater. Sci. Eng. A* **286**, 48 (2000).
68. R.B. Schwarz, *Mater. Sci. Forum* **269–272**, 665 (1998).
69. H. Gleiter, *Acta Metall.* **16**, 455 (1968).
70. K. Differt, U. Essmann, H. Mughrabi, *Phys. Status Solidi A* **104**, 95 (1987).
71. D. Raabe, S. Ohsaki, K. Hono, *Acta Mater.* **57**, 5254 (2009).
72. X. Sauvage, C. Genevois, G. Da Costa, V. Pantsyrny, *Scripta Mater.* **61**, 660 (2009).
73. X. Sauvage, A. Guillet, D. Blavette, L. Thilly, F. Lecouturier, *Scripta Mater.* **46**, 459 (2002).
74. D. Raabe, U. Hangen, *Mater. Lett.* **22**, 155 (1995).
75. D. Raabe, U. Hangen, *J. Mater. Res.* **10**, 3050 (1995).
76. T.L. Wang, J.H. Li, K.P. Tai, B.X. Liu, *Scripta Mater.* **57**, 157 (2007).
77. J. Koike, D.M. Parkin, M. Nastasi, *Philos. Mag. Lett.* **62**, 257 (1990).
78. D.A. Rigney, X.Y. Fu, J.E. Hammerberg, B.L. Holian, M.L. Falk, *Scripta Mater.* **49**, 977 (2003).
79. M. Moseler, P. Gumbsch, C. Casiraghi, A. Ferrari, J. Robertson, *Science* **309**, 1545 (2005).
80. H.-J. Kim, A. Emge, R. Winter, P. Keightley, W.-K. Kim, M.L. Falk, D.A. Rigney, *Acta Mater.* **57**, 5270 (2009). ☐